LAWRENCE
LIVERMORE
NATIONAL
LABORATORY

LLNL-CONF-610853

Preserving Spherical Symmetry in Axisymmetric Coordinates for Diffusion

T. A. Brunner, T. V. Kolev, T. S. Bailey, A. T. Till

January 16, 2013

Mathematics & Computation 2013
Sun Valle, ID, United States
May 5, 2013 through May 9, 2013

Disclaimer

International Conference on Mathematics and Computational Methods Applied to Nuclear Science & Engineering (M&C 2013)
Sun Valley, Idaho, USA, May 5-9, 2013, on CD-ROM, American Nuclear Society, LaGrange Park, IL (2013)

PRESERVING SPHERICAL SYMMETRY IN AXISYMMETRIC COORDINATES FOR DIFFUSION PROBLEMS

Thomas A. Brunner, Tzanio V. Kolev, and Teresa S. Bailey
Lawrence Livermore National Laboratory
7000 East Ave, Livermore, CA 94550
brunner6@llnl.gov, kolev1@llnl.gov, bailey42@llnl.gov

Andrew T. Till
Texas A&M University
337 Zachry Engineering Bldg., 3133 TAMU
College Station, TX 77843
attom@tamu.edu

ABSTRACT

Persevering symmetric solutions, even in the under-converged limit, is important to the robustness of production simulation codes. We explore the symmetry preservation in both a continuous nodal and a mixed finite element method. In their standard formulation, neither method preserves spherical solution symmetry in axisymmetric (RZ) coordinates. We propose two methods, one for each family of finite elements, that recover spherical symmetry for low-order finite elements on linear or curvilinear meshes. This is a first step toward understanding achieving symmetry for higher-order elements.

Key Words: spherical symmetry, finite element, axisymmetric, diffusion

1. INTRODUCTION

Recently when investigating the performance of indirect drive inertial confinement fusion (ICF) capsules, we discovered that sometimes, even for a perfectly symmetric drive, the capsule simulations did not implode symmetrically. This unphysical behavior in the simulation was tracked down to an asymmetry in the radiation diffusion solution. However, the asymmetry only showed itself for one of our axisymmetric (RZ) spatial discretizations [1] of the diffusion equation, while our other discretization [2] was insulated from this asymmetric behavior. In these ICF studies, it is important to know that we can perfectly implode a spherical capsule, so that calculated asymmetries can be attributed to physical perturbations that we will observe in an experiment, not numerical imperfections that will only appear in a simulation.

In this paper, we outline several families of axisymmetric diffusion discretizations. Some of the variations on the methods have been influenced by previous work in the fields of radiation diffusion and hydrodynamics. We then study the symmetry preservation of the methods, define some metrics to guide what we mean by symmetry preservation, and note common threads underlying the methods that do preserve spherical symmetry.

We also note that when the flaw in the diffusion spatial discretizations was discovered, we tried using axisymmetric, deterministic transport methods on the same problems. None of the existing transport methods we tried were able to preserve symmetry. We hope that our work on symmetry-preserving diffusion methods will lead to improvements for axisymmetric transport discretizations.

LLNL-CONF-610853

Table I. Coefficients specific boundary conditions in the general Eq. 2 or Eq. 5.

Boundary Condition	$\mathcal{A}$	$\mathcal{B}$	$\mathcal{C}$	Notes
Dirichlet: E	1	0	E_0	
Dirichlet: $\hat{\mathbf{n}} \cdot \mathbf{F}$	0	1	$\hat{\mathbf{n}} \cdot \mathbf{F}_0$	reflection when $\hat{\mathbf{n}} \cdot \mathbf{F}_0 = 0$
Robin: Net incoming partial flux	$1/2$	1	$2F_{\text{in}}$	vacuum when $F_{\text{in}} = 0$

2. TWO FORMS OF STEADY-STATE DIFFUSION

The familiar form of the steady-state diffusion with boundary conditions is

$$-\nabla \cdot \frac{c}{3\sigma_t}\nabla E + c\sigma_a E = S \qquad \text{on a domain } \Omega, \text{ and} \tag{1}$$

$$\mathcal{A}cE + \mathcal{B}c\hat{\mathbf{n}} \cdot \frac{\nabla E}{3\sigma_t} = \mathcal{C} \qquad \text{on the boundary } \partial\Omega, \tag{2}$$

and where E is the energy density in units of energy per volume, c is the speed of the particles, σ_x is either the absorption (a) or total (t) cross section with units of inverse length, and $\hat{\mathbf{n}}$ is the outward unit normal on the surface of the domain. Table I lists the factors $\mathcal{A}$, $\mathcal{B}$, and $\mathcal{C}$ for a variety of different boundary conditions. In general $\mathcal{A}$ and $\mathcal{B}$ are non-negative constants that depend only the type of the condition. The value $\mathcal{C}$ is also non-negative, but can be a function of position.

It is also possible to rewrite Eq. 1 as two first order equations, namely

$$\nabla \cdot \mathbf{F} = -c\sigma_a E + S \qquad \text{and} \tag{3}$$

$$\nabla \frac{c}{3} E = -\sigma_t \mathbf{F} \qquad \text{on } \Omega, \text{ and} \tag{4}$$

$$\mathcal{A}cE - \mathcal{B}\hat{\mathbf{n}} \cdot \mathbf{F} = \mathcal{C} \qquad \text{on } \partial\Omega, \tag{5}$$

where $\mathbf{F}$ is the energy flux in units of power per area.

It is these two sets of equations, Eqs. 1-2 and Eqs. 3-5 that will serve as the basis for the two families of discretizations. As they stand, the equations are valid in all geometries. But in many problems, we wish to exploit the symmetry of the physical system to reduce our computational costs. When there is cylindrical symmetry, solving the equations in axisymmetric, or cylindrical, coordinates and dropping the angular dependence can prove profitable. In this coordinate system, the gradient operator looks much like it does for the two-dimensional Cartesian coordinate system, namely

$$\nabla_{RZ} f = \frac{\partial f}{\partial r}\hat{\mathbf{e}}_r + \frac{\partial f}{\partial z}\hat{\mathbf{e}}_z = \nabla_{XY} f, \tag{6}$$

where the RZ or XY subscript denotes the coordinate system, while operators without a subscript are understood to be in 3D. The divergence operator is a little different. It can be written in several forms, including one that looks like a Cartesian divergence plus an extra term, or

$$\nabla_{RZ} \cdot \mathbf{A} = \frac{1}{r}\frac{\partial\, rA_r}{\partial r} + \frac{\partial A_z}{\partial z} = \frac{\partial A_r}{\partial r} + \frac{A_r}{r} + \frac{\partial A_z}{\partial z} = \nabla_{XY} \cdot \mathbf{A} + \frac{A_r}{r}. \tag{7}$$

It will be necessary to use this expansion below to solve the RZ system with the different options below.

3. TWO FAMILIES OF FINITE ELEMENT METHODS

We apply a finite element methodology to discretize the diffusion equations. Typically when deriving the finite element method, the unknowns are expanded in terms of basis functions and inserted into the equations. The equations are then multiplied by a weight function, usually one of the basis functions for a Galerkin method, and then integrated over the volume of the domain Ω. These integrals, which define an inner product, can be written in a compact form as

$$(u,v)_\Omega = \int_\Omega uv \,\mathrm{d}V = 2\pi \int_\Gamma ruv \,\mathrm{d}r\,\mathrm{d}z = 2\pi \sum_{\text{zones}} \int_{\Gamma_z} ruv \,\mathrm{d}r\,\mathrm{d}z, \tag{8}$$

$$(\mathbf{u},\mathbf{v})_\Omega = \int_\Omega \mathbf{u}\cdot\mathbf{v} \,\mathrm{d}V = 2\pi \int_\Gamma r\mathbf{u}\cdot\mathbf{v} \,\mathrm{d}r\,\mathrm{d}z = 2\pi \sum_{\text{zones}} \int_{\Gamma_z} r\mathbf{u}\cdot\mathbf{v} \,\mathrm{d}r\,\mathrm{d}z, \text{ and} \tag{9}$$

$$(u,v)_{\partial\Omega} = \int_{\partial\Omega} uv \,\mathrm{d}A = 2\pi \int_{\partial\Gamma} ruv \,\mathrm{d}l = 2\pi \sum_{\text{boundary faces}} \int_{\partial\Gamma_f} ruv \,\mathrm{d}l, \tag{10}$$

where each integral over the domain is actually performed as a sum of integrals over each zone. We have also simplified to the two dimensional axisymmetric case where we can integrate over the azimuthal direction. This reduces the integrals to the projection of Ω onto the two-dimensional RZ plane, Γ. The outside surface of the domain Ω is $\partial\Omega$ and $\partial\Gamma$ is the projection of $\partial\Omega$ into the RZ plane.

The hydrodynamics community [3,4] has noticed that integrating some of the equations only in the RZ plane with so-called "area weighting" preserves spherical symmetry exactly for the Euler equations. Area weighting essentially changes the weight function in the integrals above to be the basis function divided by the radius, and leads to integrals only over the RZ plane, or

$$(u,v)_\Gamma = \int_\Gamma uv \,\mathrm{d}r\,\mathrm{d}z = \sum_{\text{zones}} \int_{\Gamma_z} uv \,\mathrm{d}r\,\mathrm{d}z, \tag{11}$$

$$(\mathbf{u},\mathbf{v})_\Gamma = \int_\Gamma \mathbf{u}\cdot\mathbf{v} \,\mathrm{d}r\,\mathrm{d}z = \sum_{\text{zones}} \int_{\Gamma_z} \mathbf{u}\cdot\mathbf{v} \,\mathrm{d}r\,\mathrm{d}z, \text{ and} \tag{12}$$

$$(u,v)_{\partial\Gamma} = \int_{\partial\Gamma} uv \,\mathrm{d}l = \sum_{\text{boundary faces}} \int_{\partial\Gamma_f} uv \,\mathrm{d}l. \tag{13}$$

We will explore using both the volume and area weighting forms when developing our finite element methods below. Typically only the hydrodynamics momentum equation is area weighted while the energy equation is volume weighted. This corresponds to volume weighting Eq. 3 and area weighting Eq. 4, but this strategy has no direct correlation when discretizing Eq. 1. Also inspired by the hydrodynamics community, Palmer has developed a diffusion method [2] that preserves spherical symmetry. One of the costs of doing this area weighting, however, is that the global matrix becomes asymmetric because the weight and basis functions are essentially different.*

3.1. Continuous nodal discretizations of the second order equation for E

Eq. 1 is the standard diffusion equation and is often discretized using bilinear continuous nodal elements [5,1]. We will present two related discretizations here based on a Galerkin finite element method. We first

*The vocabulary can be confusing because the matrix has one type of symmetry and the solution has another type of symmetry. For the most part, we refer to "matrix symmetry" for the matrix, and either "solution symmetry" or simply "symmetry" to mean the solution symmetry.

approximate E as

$$E(r,z) = \sum_j w_j(r,z) E_j, \tag{14}$$

where for the lowest order (1), w_j is the usual continuous, bilinear finite element and E_j is the value of $E(r,z)$ at node j. For higher orders, this is biquadratic, bicubic, etc., with multiple support points j within a zone in addition to the nodes.

3.1.1. A volume-weighted continuous finite element discretization

If we insert Eq. 14 into Eq. 1, multiply by a weight function w_i, and integrate over the volume of the mesh we get

$$-\int_\Omega w_i \nabla \cdot \frac{1}{3\sigma_t} \nabla \sum_j w_j E_j \, \mathrm{d}V + \int_\Omega w_i \sigma_a \sum_j w_j E_j \, \mathrm{d}V = \int_\Omega w_i \frac{S}{c} \, \mathrm{d}V \tag{15}$$

We can rewrite this using our compact notation as

$$-(w, \nabla \cdot \frac{1}{3\sigma_t} \nabla w)_\Omega \mathcal{E} + (w, \sigma_a w)_\Omega \mathcal{E} = (w, \frac{S}{c})_\Omega, \tag{16}$$

where $\mathcal{E}$ is the vector of unknowns E_j and w is a vector of the basis functions. The notation $(w, \sigma_a w)_\Omega$ is a sum of volume integrals over each zone, as in Eq. 8. Manipulating Eq. 16 and applying the boundary conditions in Eq. 2 results in

$$\left[\left(\frac{1}{3\sigma_t} \nabla w, \nabla w \right)_\Omega + (\sigma_a w, w)_\Omega + \left(w, \frac{\mathcal{A}}{\mathcal{B}} w \right)_{\partial\Omega} \right] \mathcal{E} = \left(w, \frac{S}{c} \right)_\Omega + \left(w, \frac{\mathcal{C}}{c\mathcal{B}} \right)_{\partial\Omega}, \tag{17}$$

which is is valid in any coordinate system. Specializing to the two-dimensional RZ case, we get

$$\left[\left(\frac{r}{3\sigma_t} \nabla w, \nabla w \right)_\Gamma + (r\sigma_a w, w)_\Gamma + \left(rw, \frac{\mathcal{A}}{\mathcal{B}} w \right)_{\partial\Gamma} \right] \mathcal{E} = \left(rw, \frac{S}{c} \right)_\Gamma + \left(rw, \frac{\mathcal{C}}{c\mathcal{B}} \right)_{\partial\Gamma}. \tag{18}$$

This is the standard continuous Galerkin finite element discretization. Eq. 18 results in a symmetric matrix, but the magnitude of the rows and columns are proportional to the radius of the zones around the node. When Dirichlet boundary conditions are applied, $\mathcal{B} = 0$, and the equations appear invalid. In this case, we zero the elements in the matrix row for the affected unknowns, except for the diagonal that we set to one. The right hand side then gets the exact value on the boundary. We also use this procedure for all discretizations below.

More importantly, if we look at the contribution from a single zone to the global matrix in Eq. 18, it depends on both its shape and its position. Or rather, an arbitrary translation or rotation of the zone will change the coefficient matrix. In contrast with Cartesian coordinates, where zone integrals in Eq. 17 depend only on the zone's shape. This is a key reason why symmetry is not preserved in the solution.

3.1.2. An area-weighted continuous finite element discretization

Before using the area-weighted inner products, we must first expand the divergence term in Eq. 1 using Eq. 7 to get

$$-\nabla_{XY} \cdot \frac{1}{3\sigma_t} \nabla_{XY} E - \frac{1}{r 3\sigma_t} \frac{\partial E}{\partial r} + \sigma_a E = \frac{S}{c}. \tag{19}$$

Now we multiply by a test function, and integrate over the RZ plane without the factor of r,

$$-\left(w, \nabla_{XY} \cdot \frac{1}{3\sigma_t} \nabla_{XY} w\right)_\Gamma \mathcal{E} - \left(w, \frac{1}{r 3\sigma_t} \frac{\partial w}{\partial r}\right)_\Gamma \mathcal{E} + (w, \sigma_a w)_\Gamma \mathcal{E} = \left(w, \frac{S}{c}\right)_\Gamma \tag{20}$$

After integrating by parts and applying the boundary conditions in Eq. 2, we get

$$\begin{aligned}\left[\left(\nabla_{XY} w, \frac{1}{3\sigma_t} \nabla_{XY} w\right)_\Gamma - \left(w, \frac{1}{r 3\sigma_t} \frac{\partial w}{\partial r}\right)_\Gamma + (w, \sigma_a w)_\Gamma + \left(w, \frac{\mathcal{A}}{\mathcal{B}} w\right)_{\partial\Gamma}\right] \mathcal{E} \\ = \left(w, \frac{S}{c}\right)_\Gamma + \left(w, \frac{\mathcal{C}}{c\mathcal{B}}\right)_{\partial\Gamma}\end{aligned} \tag{21}$$

Eq. 21 looks exactly like the diffusion equation in 2D Cartesian coordinates, but with an extra term. This second term is what destroys the symmetry of the matrix. As in Eq. 18, each zonal matrix depends on the position of the zone as well as its shape, again because of the second term.

3.2. Mixed finite elements for E and F

In coupled radiation hydrodynamic problems, the material properties are usually zone-centered [3,6] (or even arbitrary, higher-order discontinuous [4]). We are interested in exploring the use of such discretizations for E as well, where the energy is represented by a high-order function inside each zone, but is generally discontinuous between different zones In this case, it is possible to use the Raviart-Thomas elements [7] to discretize the flux **F**. These elements have been extended to higher orders [8], and are used to discretize Eqs. 3-4 directly [9,10]. This discretization can be difficult to solve, however, because resulting operator has a large near-null space. The operator's large near-null space is due to the fact that it is a mimetic discretization [11], meaning it preserves certain continuous vector identities in the discontinuous equations. In this case, the vector identity $\nabla \cdot \nabla \times \mathbf{A} = 0$ is preserved in the discrete case for any function **A**, but errors in the solution of this form are not damped when solving the linear equation, unless a preconditioner is specifically designed for the resultant system [12,13,14].

We will use an arbitrary-order extension to the Raviart-Thomas elements to discretize **F** and E using

$$\mathbf{F}(r,z) = \sum_f \mathbf{v}_f(r,z) F_f \quad \text{and} \quad E(r,z) = \sum_j u_j(r,z) E_j \tag{22}$$

where $\mathbf{v}_f$ is the face-centered basis function for face f, and F_f is the net flux density through that face, and within a zone u_j is a discontinuous basis function. As with the continuous case, these can be of arbitrary order, with more basis functions within each face and zone as the order increases. At lowest order (0), u_j is piesewise constant on the zone and $\mathbf{v}_f$ has a constant normal to the face.

3.2.1. Volume weighted mixed equations

We start with Eq. 3, which is the zeroth angular moment of the Boltzmann transport equation and a statement of energy conservation, and Eq. 4, which is the first angular moment of the transport equation and a statement of momentum or flux conservation. We multiply the first equation with a u weight function (since it is a scalar equation) and the second equation with a **v** weight function (since it is a vector equation) to get

$$(u, \nabla \cdot \mathbf{v})_\Omega \mathcal{F} = -(u, c\sigma_a u)_\Omega \mathcal{E} + (u, S)_\Omega \tag{23}$$

$$(\mathbf{v}, c\nabla u)_\Omega \mathcal{E} = -(\mathbf{v}, 3\sigma_t \mathbf{v})_\Omega \mathcal{F}, \tag{24}$$

where $\mathcal{F}$ is a vector of the unknowns for the flux, and $\mathcal{E}$ is the vector of unknowns for the energy density. We will use integration by parts on the first term in Eq. 24 to eliminate the gradients of u, and then apply the boundary conditions Eq. 5 to get

$$(u, c\sigma_a u)_\Omega \mathcal{E} + (u, \nabla \cdot \mathbf{v})_\Omega \mathcal{F} = (u, S)_\Omega \tag{25}$$

$$(\nabla \cdot \mathbf{v}, cu)_\Omega \mathcal{E} - \left[(\mathbf{v}, 3\sigma_t \mathbf{v})_\Omega + \left(\hat{\mathbf{n}} \cdot \mathbf{v}, \frac{\mathcal{B}}{\mathcal{A}} \hat{\mathbf{n}} \cdot \mathbf{v}\right)_{\partial\Omega}\right] \mathcal{F} = \left(\hat{\mathbf{n}} \cdot \mathbf{v}, \frac{\mathcal{C}}{\mathcal{A}}\right)_{\partial\Omega}. \tag{26}$$

These two equations are valid for both the Cartesian and the axisymmetric geometries. Expanding the divergence terms using Eq. 7 since the basis functions are only defined with Cartesian operators, and explicitly including the radius gives us

$$(rcu, \sigma_a u)_\Gamma \mathcal{E} + (u, r\nabla_{XY} \cdot \mathbf{v} + v_r)_\Gamma \mathcal{F} = (ru, S)_\Gamma \tag{27}$$

$$-(r\nabla_{XY} \cdot \mathbf{v} + v_r, cu)_\Gamma \mathcal{E} + \left[(r\mathbf{v}, 3\sigma_t \mathbf{v})_\Gamma + \left(r\hat{\mathbf{n}} \cdot \mathbf{v}, \frac{\mathcal{B}}{\mathcal{A}} \hat{\mathbf{n}} \cdot \mathbf{v}\right)_{\partial\Gamma}\right] \mathcal{F} = -\left(r\hat{\mathbf{n}} \cdot \mathbf{v}, \frac{\mathcal{C}}{\mathcal{A}}\right)_{\partial\Gamma}. \tag{28}$$

The mass matrix in Eq. (27) is block-diagonal, and we can easily invert it locally for each zone and eliminate $\mathcal{E}$ from Eq. 28 after we construct the zone-local finite element sub-matrices. This gives us one equation for the flux, namely

$$\left[(r\nabla_{XY} \cdot \mathbf{v} + v_r, cu)_\Gamma (ru, c\sigma_a u)_\Gamma^{-1} (u, r\nabla_{XY} \cdot \mathbf{v} + v_r)_\Gamma + (r\mathbf{v}, 3\sigma_t \mathbf{v})_\Gamma + \left(r\hat{\mathbf{n}} \cdot \mathbf{v}, \frac{\mathcal{B}}{\mathcal{A}} \hat{\mathbf{n}} \cdot \mathbf{v}\right)_{\partial\Gamma}\right] \mathcal{F}$$
$$= (r\nabla_{XY} \cdot \mathbf{v} + v_r, cu)_\Gamma (ru, c\sigma_a u)_\Gamma^{-1} (ru, S)_\Gamma - \left(r\hat{\mathbf{n}} \cdot \mathbf{v}, \frac{\mathcal{C}}{\mathcal{A}}\right)_{\partial\Gamma}. \tag{29}$$

This equation produces a symmetric coefficient matrix, and again each zone's sub matrix depends on its position as well as its shape.

3.2.2. Area weighted mixed equations

Again, we start with Eq. 3 and Eq. 4, but immediately expand the divergence terms using Eq. 7, which gives us

$$\nabla_{XY} \cdot \mathbf{F} + \frac{F_r}{r} = -c\sigma_a E + S \tag{30}$$

$$c\nabla E = -3\sigma_t \mathbf{F}. \tag{31}$$

We now again apply the finite element machinery on this equation, but only integrate over the RZ plane leaving out the factor of r in the integrals. Alternatively, it is possible to view this as a Petrov-Galerkin method where the weight functions are the basis functions divided by r. This gives us the mixed equations

$$(u, c\sigma_a u)_\Gamma \mathcal{E} + (u, \nabla_{XY} \cdot \mathbf{v})_\Gamma \mathcal{F} + \left(u, \frac{v_r}{r}\right)_\Gamma \mathcal{F} = (u, S)_\Gamma \tag{32}$$

$$-(\nabla_{XY} \cdot \mathbf{v}, cu)_\Gamma \mathcal{E} + \left[(\mathbf{v}, 3\sigma_t \mathbf{v})_\Gamma + \left(\hat{\mathbf{n}} \cdot \mathbf{v}, \frac{\mathcal{B}}{\mathcal{A}} \hat{\mathbf{n}} \cdot \mathbf{v}\right)_{\partial\Gamma}\right] \mathcal{F} = -\left(\hat{\mathbf{n}} \cdot \mathbf{v}, \frac{\mathcal{C}}{\mathcal{A}}\right)_{\partial\Gamma}. \tag{33}$$

We can again eliminate $\mathcal{E}$ to get

$$\left[(\nabla_{XY} \cdot \mathbf{v}, cu)_\Gamma (u, c\sigma_a u)_\Gamma^{-1} \left(u, \nabla_{XY} \cdot \mathbf{v} + \frac{v_r}{r}\right)_\Gamma + (\mathbf{v}, 3\sigma_t \mathbf{v})_\Gamma + \left(\hat{\mathbf{n}} \cdot \mathbf{v}, \frac{\mathcal{B}}{\mathcal{A}} \hat{\mathbf{n}} \cdot \mathbf{v}\right)_{\partial\Gamma}\right] \mathcal{F}$$
$$= (\nabla_{XY} \cdot \mathbf{v}, cu)_\Gamma (u, c\sigma_a u)_\Gamma^{-1} (u, S)_\Gamma - \left(\hat{\mathbf{n}} \cdot \mathbf{v}, \frac{\mathcal{C}}{\mathcal{A}}\right)_{\partial\Gamma}. \tag{34}$$

This set of equations is non-symmetric. But interestingly Eq. 33 is exactly the same as the 2D Cartesian equation and is independent of r, unlike the other methods outlined in this paper. Essentially $\mathcal{F}$ computed from the gradient of $\mathcal{E}$ in this equation is the same in both Cartesian and cylindrical geometries. In deriving Palmer's method [2], some very similar operations are preformed. This also makes the zonal sub-matrix contributions from Eq. 33 independent of zone position, unlike the other methods presented so far.

3.2.3. Mixed weightings for the mixed equations

Similar to the hydrodynamics community, we have also considered the idea of choosing a different weighting, either volume or area, for each equation in the mixed formulation. If we use the volume weighted energy equation, Eq. 27, to eliminate $\mathcal{E}$ in the area-weighted flux equation, Eq. 33, we get

$$\left[(\nabla_{XY} \cdot \mathbf{v}, cu)_\Gamma \, (ru, c\sigma_a u)_\Gamma^{-1} \, (u, r\nabla_{XY} \cdot \mathbf{v} + v_r)_\Gamma + (\mathbf{v}, 3\sigma_t \mathbf{v})_\Gamma + \left(\hat{\mathbf{n}} \cdot \mathbf{v}, \frac{\mathcal{B}}{\mathcal{A}} \hat{\mathbf{n}} \cdot \mathbf{v} \right)_{\partial\Gamma} \right] \mathcal{F} = (\nabla_{XY} \cdot \mathbf{v}, cu)_\Gamma \, (ru, c\sigma_a u)_\Gamma^{-1} \, (ru, S)_\Gamma - \left(\hat{\mathbf{n}} \cdot \mathbf{v}, \frac{\mathcal{C}}{\mathcal{A}} \right)_{\partial\Gamma}. \quad (35)$$

This equation also produces an asymmetric matrix, but computing the flux from the gradient of the energy density (Eq. 33) only depends on the zone shape. In a coupled radiation-hydrodynamics code, this form may lead to more consistent coupling terms in the energy equation.

3.2.4. An alternative form of the mixed finite element integrals

Eq. 29 is the usual way of expressing this formulation, but evaluating the divergence terms in RZ coordinates is problematic. Instead, we apply the divergence theorem and integrate by parts a second time on the terms that have $\nabla \cdot \mathbf{v}$. But this time, instead of doing it over the entire domain, like we did going from Eq. 24 to Eq. 26, we are going to do it for each zone's surface. Starting with Eqs. 25-26 we get

$$(u, c\sigma_a u)_\Omega \, \mathcal{E} + (u, \mathbf{v} \cdot \hat{\mathbf{n}})_{\partial\Omega_z} \, \mathcal{F} - (\nabla u, \mathbf{v})_\Omega \, \mathcal{F} = (u, S)_\Omega \quad (36)$$

$$- (\mathbf{v} \cdot \hat{\mathbf{n}}, cu)_{\partial\Omega_z} \, \mathcal{E} + (\mathbf{v}, \nabla cu)_\Omega \, \mathcal{E} - \left[(\mathbf{v}, 3\sigma_t \mathbf{v})_\Omega + \left(\hat{\mathbf{n}} \cdot \mathbf{v}, \frac{\mathcal{B}}{\mathcal{A}} \hat{\mathbf{n}} \cdot \mathbf{v} \right)_{\partial\Omega} \right] \mathcal{F} = \left(\hat{\mathbf{n}} \cdot \mathbf{v}, \frac{\mathcal{C}}{\mathcal{A}} \right)_{\partial\Omega}, \quad (37)$$

with the $\partial\Omega_z$ signifies that the integral is the sum over the faces of each zone, including all the internal ones. This implies the surface integral term is done twice, once for each zone adjacent to a given face. Eqs. 36-37 can be reduced to the RZ plane in a straightforward manner.

Interestingly, it is not possible to apply the area weighting to these equations. Without the divergence term explicitly written in terms of r, the equations become the Cartesian geometry equations. If we choose area weighting on these terms, we will get the wrong solution.

3.3. Approximating the volume integrals with an average radius

To make the volume integrals for each zone independent of r, up to a constant scaling factor, we can use a zone-averaged r in each zone's integrals. We define an average radius of the zone or face to preserve the zone volume or face area as

$$\bar{r}_z = \frac{\int_z r \, \mathrm{d}r \, \mathrm{d}z}{\int_z \mathrm{d}r \, \mathrm{d}z} \quad \text{, and} \quad \bar{r}_f = \frac{\int_f r \, \mathrm{d}l}{\int_f \mathrm{d}l}. \quad (38)$$

These averaged $\bar{r}$'s can be used in any of volume-weighted integrals in Eqs. 18, 27-29, or 36-37. When we need to evaluate the expanded divergence terms, as in Eq. 7, we also use the same value of $\bar{r}$ to divide the radial component of the vector.

4. TESTS

We compare the symmetry of the different methods using a simple test problem of a sphere modeled on a two-dimensional axisymmetric RZ mesh, where $\varrho = \sqrt{r^2 + z^2}$ and $\vartheta = \arctan r/z$ are the radius and polar angle of the sphere in sphereical coordinates. The problem geometry is shown in Fig. 1, and we solve the problem only in one quarter of the circle. We set $S = 0$, $c = 1$, $\sigma_a = 2.0$, $\sigma_t = 5.0$, and have an incoming flux of $F_{\text{in}} = 1$ on the outer surface of the sphere at $\varrho = 1$.

With this simplified problem, Eq. 1 reduces in one dimension in spherical coordinates to

$$\frac{1}{\varrho^2}\frac{\partial}{\partial\varrho}\frac{\varrho^2}{3\sigma_t}\frac{\partial}{\partial\varrho}E = \sigma_a E. \tag{39}$$

The solution of Eq. 39 with these conditions is

$$E_{\text{sphere}}(\varrho) = \frac{4F_{\text{in}}\varrho_0}{\sinh(\lambda\varrho_0) + 2D\left(\lambda\cosh(\lambda\varrho_0) - \frac{\sinh(\lambda\varrho_0)}{\varrho_0}\right)}\frac{\sinh(\lambda\varrho)}{\varrho}, \tag{40}$$

where $D = 1/3\sigma_t$. We note that $\lim_{\varrho\to\,0}\sinh(\lambda\varrho)/\varrho = \lambda$. We can also easily solve for the flux using Eq. 4.

4.1. Measuring the symmetry error

The standard L^2 error of the code solution relative to the analytic solution is our first metric of correctness. It is defined as

$$E_{L^2} = \left[\frac{\int_\Gamma r\left(E_{\text{code}} - E_{\text{analytic}}\right)^2\,\mathrm{d}r\,\mathrm{d}z}{\int_\Gamma r\,\mathrm{d}r\,\mathrm{d}z}\right]^{1/2}. \tag{41}$$

This metric was used in all cases, independent of weighting or averaging; specifically the exact radius r was always used in a volume integral, and the analytic solution was computed at every Gauss point of the numeric integration.

Most of these methods converge at the expected rate to the correct solution, and the amount of asymmetry is within the discretization error. As a result we also measure the asymmetry directly, by comparing the values of E nearest the equator (maximum r) and pole (minimum r) of the sphere at each sphere radius ϱ and normalizing by the average value at that ϱ, given by

$$M(\varrho) = \frac{|E(\varrho,\vartheta=0) - E(\varrho,\vartheta=\pi/2)|}{E_{\text{avg}}(\varrho)}, \quad \text{with} \quad E_{\text{avg}}(\varrho) = \frac{\int E_{\text{code}}(\varrho,\vartheta)\,\mathrm{d}\vartheta}{\int\,\mathrm{d}\vartheta} \tag{42}$$

We plot the the maximum of our measure of asymmetry, $\max_\varrho M(\varrho)$, at any radius in the problem. In looking at the actual solutions to understand how the symmetry was broken, we also defined a new field on the mesh,

$$E_{\text{sym}}(\varrho,\vartheta) = \frac{E_{\text{code}}(\varrho,\vartheta) - E_{\text{avg}}(\varrho)}{E_{\text{avg}}(\varrho)} \tag{43}$$

Fig 1 shows the general geometry of the problem. We always solve this problem on a quarter circle. The mesh only extends to $\varrho = 10^{-6}$; there is a very small whole in the center of the mesh, and we apply Dirichlet boundary conditions equivalent to the analytic solution on the center surface.

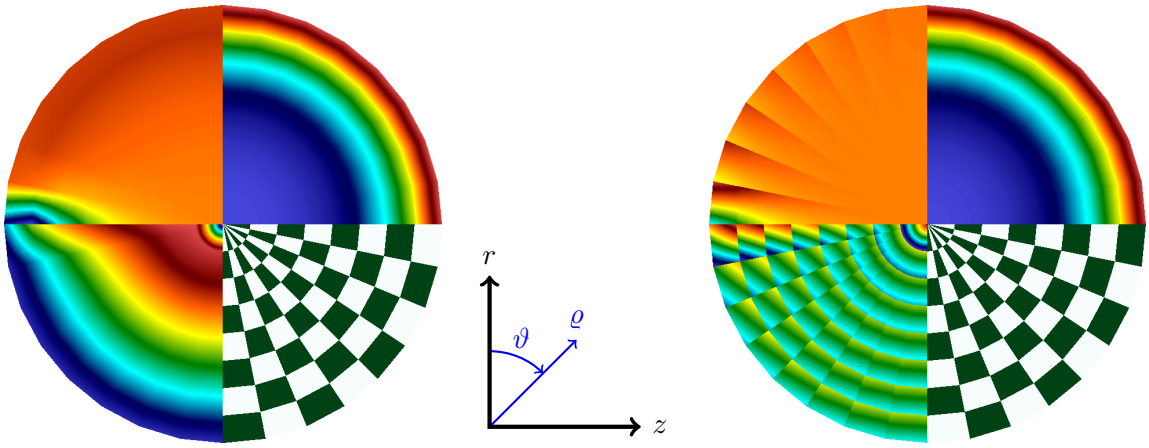

(a) Continuous FEM (b) Mixed FEM

Figure 1. The test problem with the two families of discretizations. In the upper right quarter of each subfigure is the code solution, lower right shows the mesh zones, lower left is the relative error to the analytic solution, and the upper left is the relative asymmetry in Eq. 43.

4.2. Results

Two test codes were written using the the finite element library MFEM [15,16], one for all the continuous discretizations, and another for all the continuous cases. MFEM supports arbitrary order finite elements as well as curvilinear meshes. In all cases the resulting matrices were solved using the sparse direct solver UMFPACK [17] to get as exact of a result as possible.

The various options of volume weighting, area weighting, and using averaged $\bar{r}$'s were tried in many different combinations. Finite elements of up to order three were used; The notation "E0" signifies a zeroth order (piecewise constant) representation for the energy density, E1 is bilinear, E2 is bi-quadratic and so forth. Various mesh orders were also used. M1 means straight edge meshes, M2 is bi-quadratically deformed zones, and so on. We computed results for third order meshes, but since the quadratic meshes approximated the sphere extremely well, the M3 meshes showed no improvement over the M2 ones, so they are excluded from the figures for clarity. Table II summarized the results. Figures 2-5 shows convergence rates and symmetry metrics for some interesting cases. In general, the more sides the symbol has, the higher order the polynomial representation for the energy density.

Several general trends were observed:

- For the most part all the methods that used the exact r got the expected convergence rates, namely their finite element order plus one. The exception is with linear meshes, where all methods are at best second order.
- Improving mesh order, holding everything else the same, always improves solution symmetry.
- Area weighting the continuous Eq. 21 did not restore solution symmetry.
- Using an average $\bar{r}_z$ in the continuous Eq. 18 restored solution symmetry for all element and mesh orders, but convergence was limited to second order. The error we are making in the integral of the zone by using the average radius dominates the solution error. (Fig. 3)

Table II. Summary of the results for the different methods. The radius refers to if we use the exact radius or an averaged radius in integrals. "ZMI" stands for "Zone Matrix Independence", or the property that each zone's contribution to the global matrix depends on only the zone's shape and size, but not the position, up to a scale factor. The convergence plots for some methods are skipped in the favor of space.

Eqs.	Method	Weight	Radius	Matrix Symmetry	Approx. Order	ZMI	Solution Symmetry	Fig.
18	CFEM	volume	r	yes	expected	no	no	2
18	CFEM	volume	$\bar{r}_z$	yes	$\mathcal{O}(h^2)$	yes	yes	3
21	CFEM	area	r	no	expected	no	no	
29	mixed	volume	r	yes	expected	no	E0-M1	4
29	mixed	volume	$\bar{r}_z$	yes	none	yes	no	
34	mixed	area	r	no	expected	only Eq. 33	E(0,1)-M(n)	5
35	mixed	area	r	no	expected	only Eq. 33	E(0,1)-M1	
36-37	mixed	volume	r	yes	expected	no	E0-M1	
36-37	mixed	volume	$\bar{r}_z, \bar{r}_f$	yes	expected	no	no	

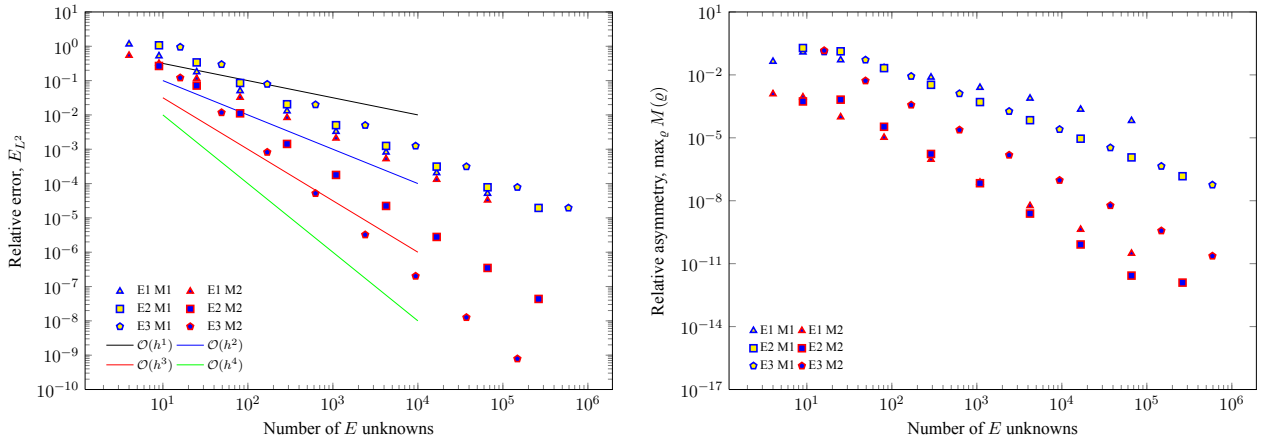

(a) L^2 convergence rate **(b) Relative asymmetry metric**

Figure 2. Convergence of the continuous finite element method with exact radius in Eq. 18. All methods converge at the expected rate, but none preserve spherical symmetry.

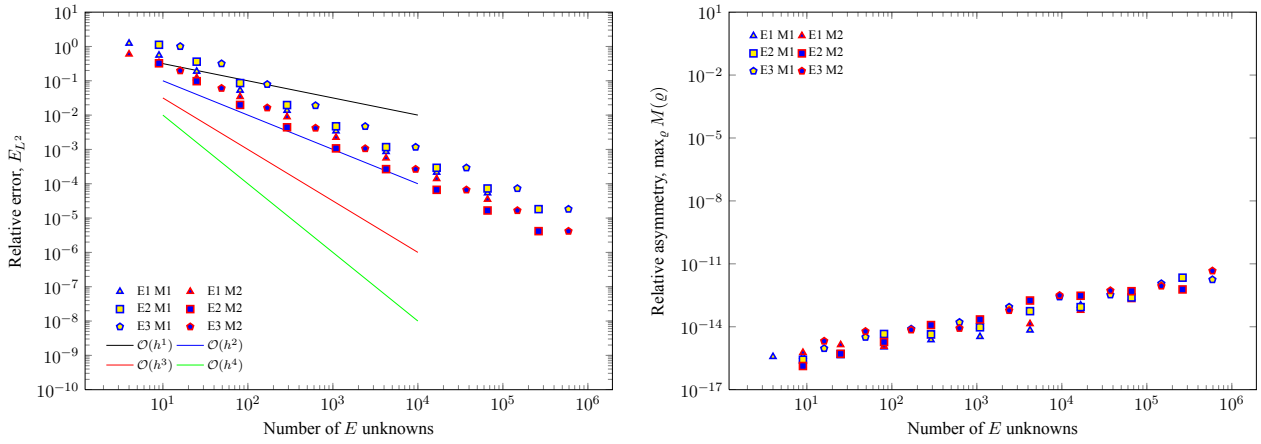

(a) L^2 convergence rate **(b) Relative asymmetry metric**

Figure 3. Convergence of the continuous finite element method with a zone averaged radius in Eq. 18. Spherical symmetry is exact to round-off, but the convergence rate is limited to second order.

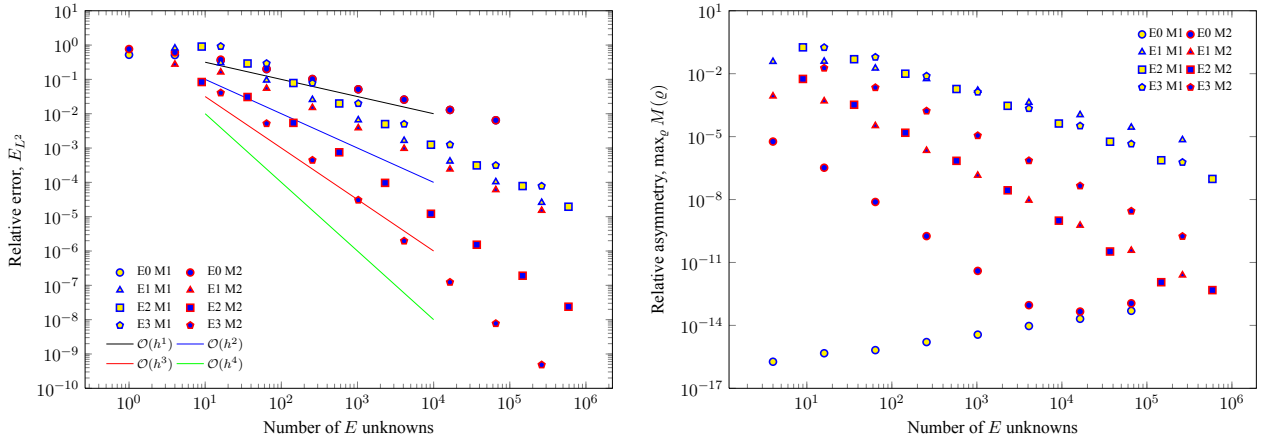

(a) L^2 convergence rate **(b) Relative asymmetry metric**

Figure 4. Convergence of the mixed finite element method with exact radius in Eq. 29. All converge at the expected rate, but without spherical symmetry, except for the lowest order method.

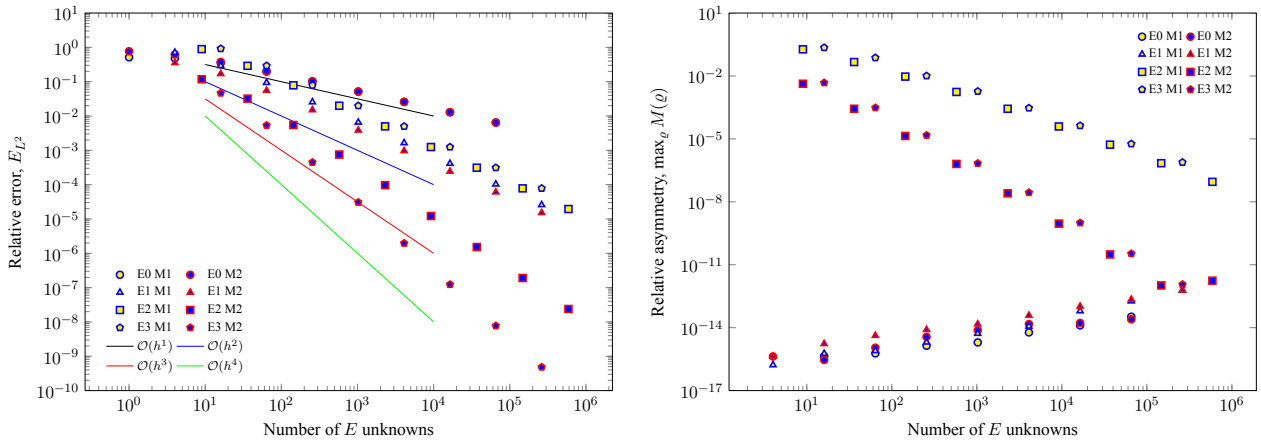

(a) L^2 convergence rate **(b) Relative asymmetry metric**

Figure 5. Convergence of the mixed finite element method area weighting in Eq. 34. All converge at the expected rate, and symmetry is preserved for piecewise constant or bilinear methods.

- The lowest order mixed finite element method always had solution symmetry, for any variations. We believe this is due to the piecewise constant basis function for the energy density. This method is likely related to one by Morel [18]. He also proves that his method always has spherical symmetry. (Fig. 4)
- Area weighting the mixed finite element Eq. 34 also restored symmetry for all mesh orders, but only for the lowest two finite element orders E0 and E1, as seen in Fig. 5. Area weighting both equations preserved solution symmetry in more cases than mixing volume and area weighting in Eq. 35, where solution symmetry was only preserved on linear meshes. (These figures are not shown to save space.)
- Using a zone average $\bar{r}_z$ in the mixed finite element Eq. 29 destroys the convergence, so is not shown. We believe this is because the implicit terms that define the flux through the face (computed using volume integrals in the zone) do not match the flux through a face from the zones on either side of the face.
- Using the alternative divergence formulation of Eqs. 36-37 produced results in the exact volume integral case indistinguishable from Fig. 4, but are not shown to save space. Using the volume averaged zone radius in the volume integrals and the area averaged radius for all the face integrals did restore convergence to second order (an improvement over using the averaged $\bar{r}_z$ in Eq. 29), but there was no solution symmetry, even for the lowest order E0.
- Higher order elements and meshes reduces the solution asymmetry quickly enough that converging the error away may be practical. With linear elements and meshes, too many levels of mesh refinement are necessary to be practical.

5. CONCLUSIONS

Preserving spherical solution symmetry is important when modeling physical systems. While many methods converge to a symmetric solution, users typically run their simulations under-resolved and the solution asymmetries can be significant.

Using a zone-averaged radius in the zone volume integrals for continuous finite element methods restored the solution symmetry. This may be due to the fact that for these cases the zonal contributions to the global

matrix are independent of zone position, up to a scale factor. But in this case, the convergence order was limited to second order.

Using area-weighting in the mixed finite elements also restored solution symmetry, just like it does with similar hydrodynamic discretizations. This comes at the cost of creating an asymmetric matrix. Here, it seemed important that the calculation of the flux from the gradient of the energy density produced a matrix that was independent of the zone position.

In our production code, the discretization that does not preserve solution symmetry is essentially an extension of a continuous nodal finite element method, extended to work on arbitrary polygons [1]. We hope to improve symmetry in that approximation by applying the zone-averaged radius. The other method [2] already used something like area-weighting, and so no enhancements are needed for it.

Using the alternative divergence form of the equations remains a promising area for future work. We also hope to better understand the circumstances of when the various methods will have solution symmetry for this diffusion system. Then we hope to apply the lessons learned to improve our discretizations of the transport equation.

ACKNOWLEDGMENTS

This work performed under the auspices of the U.S. Department of Energy by Lawrence Livermore National Laboratory under Contract DE-AC52-07NA27344. We would also like to thank ML Adams for supporting AT Till's visit to LLNL in the summer of 2012 to work on this topic.

REFERENCES

[1] T. S. Bailey, M. L. Adams, B. Yang, and M. R. Zika, "A piecewise linear finite element discretization of the diffusion equation for arbitrary polyhedral grids," *Journal of Computational Physics*, **227**, 8, pp. 3738 – 3757 (2008).

[2] T. S. Palmer, "Discretizing the diffusion equation on unstructured polygonal meshes in two dimensions," *Annals of Nuclear Energy*, **28**, 18, pp. 1851 – 1880 (2001).

[3] M. Wilkins, "Methods in computational physics," *Calculation of elastic–plastic flow*, pp. 211–263 (1964).

[4] V. Dobrev, T. Ellis, T. Kolev, and R. Rieben, "High-Order Curvilinear Finite Elements for Axisymmetric Lagrangian Hydrodynamics," *Computers & Fluids* (2012, to appear), also available as LLNL technical report LLNL-JRNL-521372.

[5] D. S. Kershaw, "Differencing of the diffusion equation in Lagrangian hydrodynamic codes," *Journal of Computational Physics*, **39**, 2, pp. 375 – 395 (1981).

[6] E. J. Caramana, , D. E. Burton, M. J. Shashkov, and P. P. Whalen, "The construction of compatible hydrodynamics algorithms utilizing conservation of total energy," *Journal of Computational Physics*, **142**, pp. 227–262 (1998).

[7] P. A. Raviart and J. M. Thomas, "A mixed finite element method for second order elliptic problems," in I. Galligani and E. Magenes, editors, "Mathematical aspects of the finite element method," Springer-Verlag, New York (1977).

[8] R. Hiptmair, "Canonical Construction of Finite Elements," *Mathematics of Computation*, **68**, 228, pp. 1325–1346 (1999).

[9] G. Chavent and J. E. Roberts, "A unified physical presentation of mixed, mixed-hybrid finite elements and standard finite difference approximations for the determination of velocities in waterflow problems," *Advances in Water Resources*, **14**, 6, pp. 329 – 348 (1991).

[10] P. B. Bochev and D. Ridzal, "Rehabilitation of the Lowest-Order Raviart-Thomas Element on Quadrilateral Grids," *SIAM J. Numer. Anal*, **47**, 1, pp. 487–507 (2008).

[11] M. Berndt, K. Lipnikov, D. Moulton, and M. Shashkov, "Convergence of mimetic finite difference discretizations of the diffusion equation," *Journal of Numerical Mathematics*, **9**, 4, pp. 265–284 (2001).

[12] R. Hiptmair and J. Xu, "Nodal Auxiliary Space Preconditioning in H(curl) and H(div) Spaces," *SIAM J. Numer. Anal.*, **45**, pp. 2483–2509 (October 2007).

[13] T. Kolev and P. Vassilevski, "Parallel Auxiliary Space AMG Solver for H(div) Problems," *SIAM J. Sci. Comp.*, **34**, 6, pp. A3079–A3098 (2012), also available as LLNL technical report LLNL-JRNL-520391.

[14] R. S. Tuminaro, J. Xu, and Y. Zhu, "Auxiliary Space Preconditioners for Mixed Finite Element Methods," in M. Bercovier, M. J. Gander, R. Kornhuber, and O. Widlund, editors, "Domain Decomposition Methods in Science and Engineering XVIII," Springer Berlin Heidelberg, *Lecture Notes in Computational Science and Engineering*, vol. 70, pp. 99–109 (2009).

[15] T. Kolev and V. Dobrev, "MFEM: Finite Element Discretization Library," `http://mfem.googlecode.com`.

[16] T. A. Brunner, "Mulard: A Multigroup Radiation Diffusion Proxy Applicaiton," `https://codesign.llnl.gov/Mulard` (2012), LLNL-CODE-574952.

[17] T. A. Davis, "Algorithm 832: UMFPACK V4.3—an unsymmetric-pattern multifrontal method," *ACM Trans. Math. Softw.*, **30**, 2, pp. 196–199 (Jun. 2004).

[18] J. Morel, R. M. Roberts, and M. J. Shashkov, "A Local Support-Operators Diffusion Discretization Scheme for Quadrilateral r-z Meshes," *Journal of Computational Physics*, **144**, 1, pp. 17 – 51 (1998).